JOURNAL OF SOLID STATE CHEMISTRY 116, 8–14 (1995)

Kinetics of Nucleation of Lead Hydroxylapatite and Preparation of Solid Solutions of Calcium–Cadmium–Lead Hydroxylapatite: An X-Ray and IR Study

P. P. Mahapatra,[1] D. S. Sarangi, and Bagmi Mishra

Post Graduate Department of Chemistry, Gangadhar Meher Autonomous College, Sambalpur 768004, India

Received February 22, 1993; in revised form July 12, 1994; accepted July 15, 1994

The Kinetics of the nucleation of lead hydroxylapatite was studied from saturated solutions of lead and phosphorus at pH ~12 and at a temperature of 37°C. The incipient phase precipitated was apatitic, and the process was one of crystal growth and perfection with time similar to Ostwald's crystal ripening process. The crystal growth and perfection phenomena is reflected from the 002 peak in XRD and the resolution of ν_s(OH) and ν_3(PO_4) vibration in the IR spectra. The solid solutions of calcium–cadmium–lead hydroxylapatite were prepared from solutions at pH ~12. The formation of the samples was confirmed by measurements of lattice constants and IR spectra. The ordered cation occupancy of 60 mole% (Cd + Pb) in the 6*h* apatite site is discussed. The existence of a hydrogen bonding mechanism in the samples of the solid solutions is observed. © 1995 Academic Press, Inc.

1. INTRODUCTION

Hydroxylapatite, $Ca_{10}(PO_4)_6(OH)_2$ (CaHA), is a major component of human bones and teeth; if synthesized artificially it is a very important biocompatible material capable of allowing various ion-exchange reactions in it, of which lead, the toxic heavy metal pollutant, is of great importance. The presence of this toxic metal in bones results in painful bone diseases (1–3), accelerating osteoporetic processes (4), and dental caries (5). Although the kinetics of the nucleation growth mechanism of CaHA is well known (6, 7), that of lead hydroxylapatite, $Pb_{10}(PO_4)_6(OH)_2$ (PbHA) has not been understood in spite of the fact that lead is a potential bone-seeker.

The studies (8–12) on CaHA, PbHA, and cadmium hydroxylapatite, $Cd_{10}(PO_4)_6(OH)_2$ (CdHA) reveal them to be isomorphous. Hence from the closeness of the ionic radii of Ca^{2+} (0.99 Å), Cd^{2+} (0.97 Å), and Pb^{2+} (1.20 Å) and the isomorphism of CaHA, CdHA, and PbHA, the formation of solid solutions among them is considered possible as a result of the simultaneous coupled substitution of both Cd and Pb in CaHA leading to the formation of solid solutions of composition: $Ca_{10-x-y}Cd_xPb_y(PO_4)_6(OH)_2$(CaCdPbHA). Engel (13) has reported the IR spectra of lead hydroxylapatite, $(Pb_{10}(PO_4)_6(OH)_2)$, oxyapatite $(Pb_{10}(PO_4)_6O)$, and lead alkaliapatites $(Pb_8M_2(PO_4)_6$ [M = Na, K, Rb, Tl]) down to 200 cm^{-1} and observed a significant difference between all these spectra. Heijligers *et al.* (14) and Bigi (15) confirmed the linear variation of a-2 and c-axis dimensions in calcium–cadmium apatites according to Vegard's law. The deviations from Vegard's law in lead hydroxylapatites have recently been observed (16, 17) and are attributed to a possible preference of Pb^{2+} ions for site (II) of the apatite structure on the basis of the cation distribution deduced from the relative intensities of suitable reflections in the powder diffractogram. The IR spectra of different cadmium apatites which are structurally related to calcium fluoroapatite have been investigated by Baran (18). The distortion effects produced by Cd^{2+} ions in these apatite lattices are discussed.

The present investigation deals with the nucleation phenomena of lead hydroxylapatite and the formation of solid solutions of CaCdPbHA studied by chemical analyses, IR, X-ray diffraction, and determination of lattice constants of the solid solutions. The occupancy of the cations in the apatite lattice is discussed from the XRD spectra.

2. EXPERIMENTAL

2.1. Nucleation

A stoichiometric solution of ammonium dihydrogen phosphate was rapidly added to a solution of lead acetate to achieve the final molar Pb/P ratio of 1.67. All solutions were prepared in CO_2-free conductivity water and maintained at pH ~12 with ethylenediamine. The reaction was carried out at 37°C in a closed 3-liter flask. N_2 gas was continuously bubbled to prevent absorption of CO_2 gas during nucleation. The flask was housed on a magnetic stirrer in order to keep the slurry in intimate contact with

[1] To whom correspondence should be addressed.

0022-4596/95 $6.00

the reaction solution for a period of 96 hr. Samples were withdrawn at fixed intervals, lyophylized, washed well with ammoniacal ice-cold double-distilled water, dried at 200°C, and analyzed complexometrically.

The samples were characterized by X-ray diffraction and IR spectra. In the XRD the scattering region between 10° and 60° 2θ was surveyed for the nucleation experiments, while that between 10° and 40° 2θ was surveyed for the solid solutions of CaCdPbHA. The 002 peak appeared sufficiently resolved for the samples in the nucleation experiment for line-breadth measurements, since it was observed qualitatively that variations in the degree of resolution of the remainder of the diffraction patterns paralleled changes in the 002 peak. The IR spectra were recorded using the KBR-pellet technique.

2.2. *Synthesis of Solid Solution*

The samples were synthesized according to the equation

$$(10 - x - y)Ca^{2+} + xCd^{2+} + yPb^{2+} + 6PO_4^{3-} + 2OH^- \rightarrow Ca_{(10-x-y)}Cd_xPb_y(PO_4)_6(OH)_2$$

by interacting at 100°C a solution of diammonium hydrogen phosphate and a mixed cation solution of Ca, Cd, and Pb nitrates added dropwise to 2 liters of boiling conductivity water maintained at pH ~12 with ethylenediamine in a 4-liter flask. Care was taken to exclude the formation of carbonate-apatites. The precipitate was aged for 2 hr under reflex, left overnight, centrifuged, washed repeatedly with 2% EDTA solution maintained at pH ~11 (19), followed by rinsing with doubly distilled water, and dried at 200°C. The homogeneity was confirmed through chemical analyses of the samples for Ca, Cd, Pb, and phosphorus complexometrically specially worked out (20), IR spectra, and X-ray spectra as reported earlier (20).

3. RESULTS AND DISCUSSION

3.1. *Nucleation of PbHA*

The results of the kinetics of nucleation of PbHA are given in Table 1. It is observed from the Pb/P g · atom ratio of 1.56 at zero hour that the initial precipitated phase is apatitic in nature. This is revealed from the shape and size of ν_{PO_4} and ν_{OH} absorptions in the IR spectra (Fig. 1), in addition to a discrete apatitic peak in the XRD at zero hour (Fig. 2) immediately after mixing. The g · atom ratio of Pb/P with time indicates a progressive increase from 1.56 to 1.64 in 96 hr. The initial phase at zero hour incorporated about 45% of the total lead. Although an uptake of phosphorus from the solution was also observed during 0–60 hr but the uptake of Pb was maximum with an increase from 51.80 wt.% to 74.75 wt.% between zero and 60 hr and remained constant thereafter. Since no differences in the IR and XRD are noticeable except in the sharpness of the XRD peak, besides the apparent

TABLE 1

Results of Chemical Analyses, the Width at One-Half Maximum Height ($\beta_{1/2}$) of the 002 XRD Peak, and Mean Crystal Size (D) of Samples during Kinetics of Nucleation of PbHA

Time (hr)	wt.% Pb	wt.% P	Pb/P	$\beta_{1/2}$ (2θ) (Å)	Mean crystal size (D) (Å)
0	51.80	4.96	1.56	0.0974	815
1	51.80	4.96	1.56	0.100	815
2	51.80	4.96	1.56	0.100	815
5	55.89	5.27	1.58	0.090	905
8	57.96	5.58	1.55	0.090	982
16	60.03	5.58	1.61	0.080	1019
24	61.20	5.74	1.62	0.080	1019
48	61.10	6.74	1.62	0.080	1022
60	74.75	6.82	1.64	—	—
72	74.75	6.82	1.64	—	—
96	74.75	6.82	1.64	0.080	1022

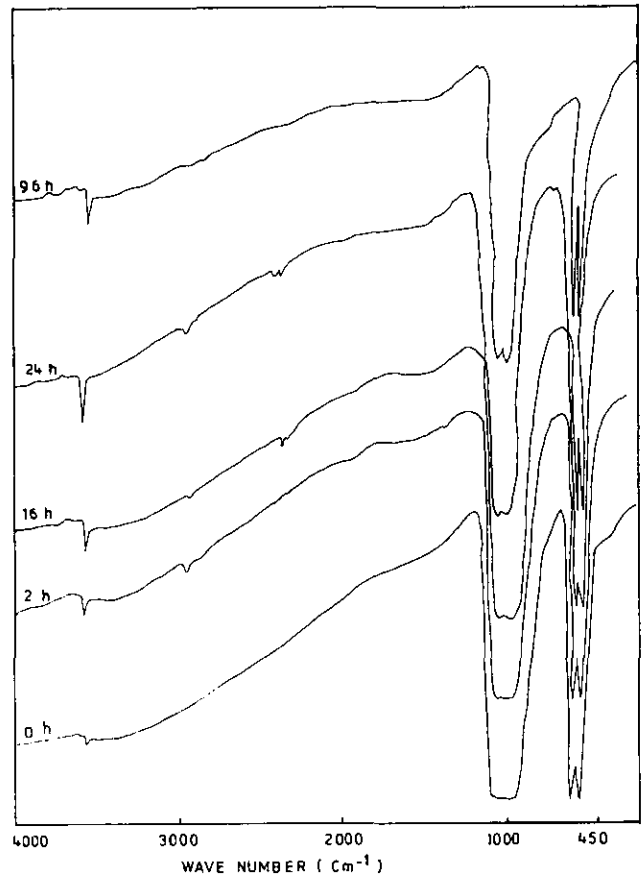

FIG. 1. Infrared spectra of samples of lead hydroxylapatite during nucleation.

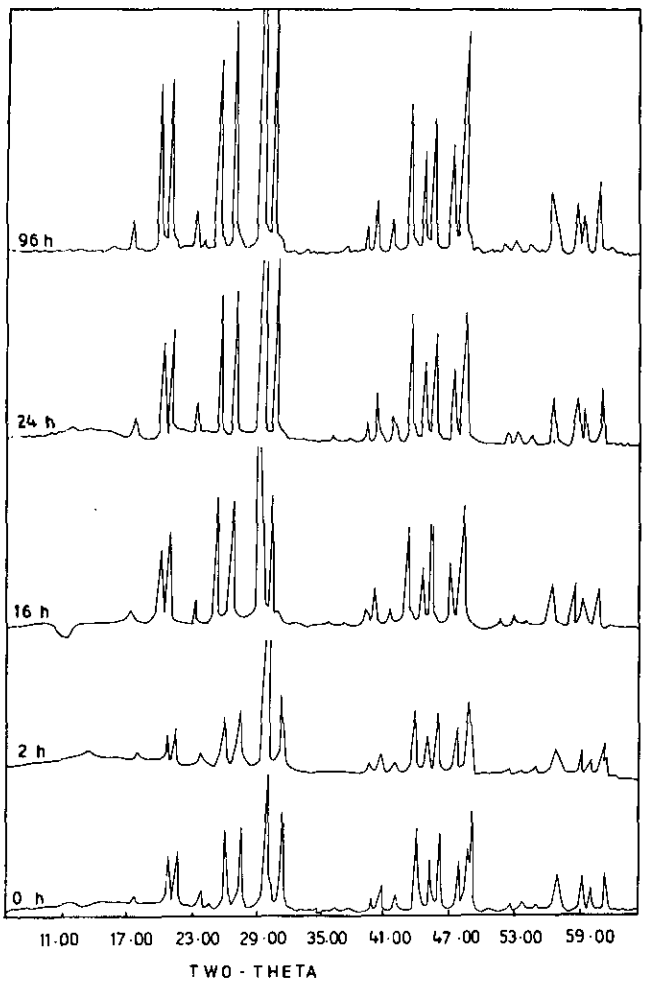

FIG. 2. X-ray diffraction patterns of samples of lead hydroxylapatite during nucleation.

resolution of the $\nu_3(PO_4)$ vibration at 96 hr and the $\nu_s(OH)$ band at 3560 cm^{-1} in the IR spectra, this is an indication of crystal growth and maturation phenomena. The initial nucleation phase being apatitic, the overall process from zero to 96 hr is one of crystal perfection and growth only with time.

The 002 peak in the XRD patterns on which the crystallinity is measured has progressed well to develop in agreement with the decrease in the solution lead level (Fig. 3) and the increase in the molar Pb/P ratio in the solid. The measurement along the 002 peak can be assumed to be proportional to changes in the magnitude of the weight fraction of the crystalline phase with time. Although apatites show different crystallization properties along the *a*- than along the *c*-axis, the width at one-half the maximum height of the 002 peak, $\beta_{1/2}$ was measured in degree 2θ. The quantity, $1/\beta_{1/2}$, is proportional to the mean crystallite size and/or degree of perfection in the direction along the *c*-axis of the crystals. Since the degree of resolution of the remainder of the diffraction peak parallels the changes in the 002 reflection, it is therefore taken as representative of the whole. The progressive sharpness of the XRD peak on the 002 reflections show the $1/\beta_{1/2}$ value equal to 1.026 at zero hour and 12.50 at 96 hr indicating thereby the ripening and growth of the apatite crystal, initially formed similarly to Ostwald's crystal growth process. The mean crystal size, *D*, at different sampling intervals was estimated from the breadth at 1/2 maximum height of the 002 diffraction peak of the samples by use of Scherrin's formula. For PbHA the mean crystal size varies around 207 Å, which means that the nuclei once formed grow slowly to final size within a span of 96 hr.

3.2. Solid Solutions of CaCdPbHA

The results of chemical analyses in Table 2 indicate formation of a solid solution of CaCdPbHA. The XRD patterns (Fig. 4) exhibit discrete peaks characteristic of apatites belonging to the $P6_3/m$ space group. The samples 1, 3, and 5 are not well resolved, perhaps due to their poor crystalline character in comparison with that of others. The results of chemical analyses and the variations in the values of lattice constants *a* and *c* determined from a least-squares fitting of several peak positions on mole% compositions of cations strongly indicate the formation of solid solutions; however, Vegard's law is not strictly obeyed (Fig. 5). Although this does not reflect upon the homogeneity in the compositions of the samples prepared over the entire compositional range it indicates a partial ordering phenomena of the cations Cd^{2+} and Pb^{2+} in the 6*h* and 4*f* sites of the apatite lattice. The ordering phenom-

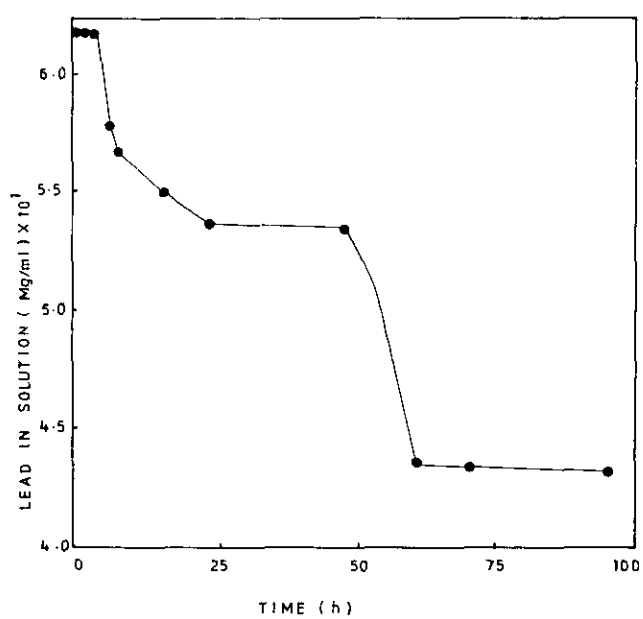

FIG. 3. Dependence of lead present in solution on time of nucleation.

TABLE 2
Chemical Analyses of Solid Solutions of Calcium–Cadmium–Lead Hydroxylapatites

No.	Molecular formula	wt.% (experimental/theoretical) Ca	Cd	Pb	P	(Ca + Cd + Pb)/P g·atom ratio
1	$Ca_8Cd_1Pb_1(PO_4)_6(OH)_2$	26.05 (25.77)	9.13 (9.03)	16.36 (16.65)	14.90 (14.93)	1.68
2	$Ca_7Cd_1Pb_2(PO_4)_6(OH)_2$	20.44 (19.88)	7.86 (7.96)	29.00 (29.36)	13.11 (13.16)	1.69
3	$Ca_6Cd_1Pb_3(PO_4)_6(OH)_2$	15.33 (15.23)	7.02 (7.12)	39.36 (39.38)	11.74 (11.76)	1.67
4	$Ca_5Cd_1Pb_4(PO_4)_6(OH)_2$	11.62 (11.48)	6.40 (6.43)	47.24 (47.48)	10.66 (10.64)	1.67
5	$Ca_4Cd_1Pb_5(PO_4)_6(OH)_2$	8.81 (8.38)	5.62 (5.87)	53.87 (54.16)	9.90 (9.71)	1.67
6	$Ca_3Cd_1Pb_6(PO_4)_6(OH)_2$	6.01 (5.78)	5.05 (5.40)	59.05 (59.78)	8.90 (8.93)	1.68
7	$Ca_2Cd_1Pb_7(PO_4)_6(OH)_2$	3.60 (3.56)	4.94 (5.00)	64.75 (64.55)	8.28 (8.27)	1.67
8	$Ca_1Cd_1Pb_8(PO_4)_6(OH)_2$	1.60 (1.66)	4.49 (4.65)	68.79 (68.66)	7.63 (7.69)	1.67
9	$Ca_7Cd_2Pb_1(PO_4)_6(OH)_2$	22.01 (22.31)	16.86 (17.07)	14.50 (15.74)	14.24 (14.11)	1.67
10	$Ca_6Cd_2Pb_1(PO_4)_6(OH)_2$	18.03 (17.31)	24.72 (24.28)	13.46 (14.42)	13.41 (13.38)	1.69
11	$Ca_4Cd_3Pb_3(PO_4)_6(OH)_2$	9.61 (9.30)	19.10 (19.57)	36.26 (36.07)	10.71 (10.79)	1.69
12	$Ca_5Cd_4Pb_1(PO_4)_6(OH)_2$	13.82 (13.71)	30.62 (30.77)	13.98 (14.18)	12.67 (12.71)	1.67
13	$Ca_2Cd_4Pb_4(PO_4)_6(OH)_2$	4.40 (4.08)	23.04 (22.91)	41.44 (42.23)	9.57 (9.46)	1.66
14	$Ca_4Cd_5Pb_1(PO_4)_6(OH)_2$	10.42 (10.45)	36.53 (36.65)	13.46 (13.51)	12.07 (12.11)	1.67
15	$Ca_3Cd_6Pb_1(PO_4)_6(OH)_2$	7.51 (7.48)	42.15 (42.00)	12.95 (12.90)	11.59 (11.57)	1.67
16	$Ca_1Cd_6Pb_3(PO_4)_6(OH)_2$	2.16 (2.06)	34.84 (34.76)	31.90 (32.04)	9.57 (9.57)	1.67
17	$Ca_2Cd_7Pb_1(PO_4)_6(OH)_2$	4.91 (4.77)	47.20 (46.88)	11.91 (12.34)	11.03 (11.07)	1.68
18	$Ca_1Cd_8Pb_1(PO_4)_6(OH)_2$	2.40 (2.29)	51.70 (51.37)	11.18 (11.83)	10.59 (10.83)	1.67

ena is indicated by the changes in the relative intensity of the reflections and their positions in the XRD spectra consequent to the alterations in the atomic distances. The peak intensity values along the 211 plane is measured since variations along this peak are most apparently affected. The peak intensity values (I/I_0), measured along the 211 reflection as peak heights above the background and expressed as percentages of the strongest line, are 100, 85, and 80 for CaHA, CdHA, and PbHA respectively. It is observed that the peak intensity values along the 211 reflection varied from 18 to 100 between compositions $Ca_8Cd_1Pb_1(PO_4)_6(OH)_2$ and $Ca_1Cd_1Pb_8(PO_4)_6(OH)_2$. A lower I/I_0 value is observed when the total (Cd + Pb) content in the samples ranged between 5 and 6 g · atoms in the compositions, viz., $Ca_4Cd_3Pb_3(PO_4)_6(OH)_2$ [I/I_0 = 19], $Ca_5Cd_4Pb_1(PO_4)_6(OH)_2$ [I/I_0 = 21], and $Ca_5Cd_1Pb_4(PO_4)_6(OH)_2$ [I/I_0 = 16], although relatively higher I/I_0 values are observed when the (Cd + Pb) content in the samples are greater than 6 g · atom. In the molecular composition $Ca_3Cd_1Pb_6(PO_4)_6(OH)_2$ a deviation to this trend is, however, observed.

The changes observed in the line widths are due to the induced structural disordered occupancy of the cations during coupled substitution of Cd and Pb in CaHA. The c/a values (Table 3) decreased up to 60 mole% incorporation of Pb and then increased. This indicates that during substitution a partial ordering occurs, viz., the Cd^{2+} and Pb^{2+} ions get statistically ordered over the 6*h* rather than the 4*f* sites. The smaller Cd that substitutes for Ca probably locates at the 6*h* site. Besides, Pb has a preference

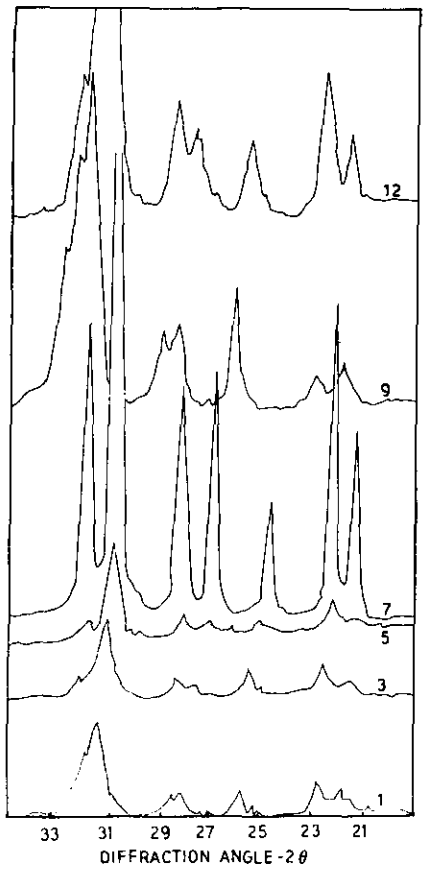

FIG. 4. X-ray diffraction patterns of samples 1, 3, 5, 7, 9, and 12 (see Table 3).

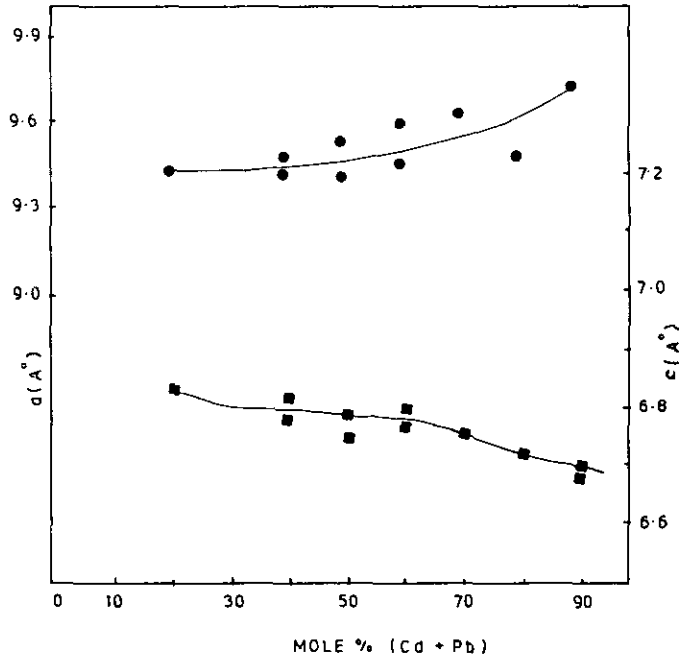

FIG. 5. Dependence of lattice constants on mole% (Cd + Pb) composition of samples of Ca Cd Pb HA.

for 6*h*. Therefore, for the total 60 mole% substitution of (Cd + Pb), the 6*h* site will be preferentially occupied over the 4*f* in the lattice.

Due to variations in the compositional parameters in the samples the phosphate vibrations, the point group symmetry, and the spectral positions are affected in the

TABLE 3
Lattice Parameters *a* and *c*, Cell Volume, and OH···O Distance of Samples of CaHA, CdHA, PbHA, and Solid Solutions of CaCdPbHA

No.	Molecular formula	Lattice constants (Å)		*c*/*a*	Unit cell volume (Å^3)	OH···O distance (Å)
		c	*a*			
1	$Ca_8Cd_1Pb_1(PO_4)_6(OH)_2$	6.84	9.435	0.724	527.30	3.104
2	$Ca_6Cd_1Pb_3(PO_4)_6(OH)_2$	6.825	9.485	0.719	531.73	3.072
3	$Ca_5Cd_1Pb_4(PO_4)_6(OH)_2$	6.797	9.537	0.712	535.37	3.072
4	$Ca_4Cd_1Pb_5(PO_4)_6(OH)_2$	6.77	9.595	0.705	539.75	2.965
5	$Ca_3Cd_1Pb_6(PO_4)_6(OH)_2$	6.775	9.623	0.701	541.70	2.965
6	$Ca_1Cd_1Pb_8(PO_4)_6(OH)_2$	7.07	9.717	0.727	578.09	3.11
7	$Ca_6Cd_3Pb_1(PO_4)_6(OH)_2$	6.782	9.415	0.720	520.61	3.072
8	$Ca_4Cd_3Pb_3(PO_4)_6(OH)_2$	6.80	9.455	0.719	526.44	3.043
9	$Ca_5Cd_4Pb_1(PO_4)_6(OH)_2$	6.75	9.412	0.717	517.82	2.989
10	$Ca_2Cd_4Pb_4(PO_4)_6(OH)_2$	6.72	9.475	0.709	522.45	3.043
11	$Ca_1Cd_6Pb_3(PO_4)_6(OH)_2$	6.70	9.416	0.711	514.43	2.965
12	$Ca_1Cd_8Pb_1(PO_4)_6(OH)_2$	6.68	9.39	0.711	510.06	3.07
13	$Ca_{10}(PO_4)_6(OH)_2$	6.86	9.42	0.728	527.17	3.068
14	$Cd_{10}(PO_4)_6(OH)_2$	6.614	9.01	0.734	464.99	2.955
15	$Pb_{10}(PO_4)_6(OH)_2$	7.241	9.871	0.733	611.01	3.061

TABLE 4
Frequency (in cm^{-1}) and Assignments of the Bands in the IR Spectra of Samples of Solid Solutions of Calcium–Cadmium–Lead Hydroxylapatites

		PO_4 (cm^{-1})				Hydroxyl (cm^{-1})	
No.	Molecular formula	ν_1	ν_2	ν_3	ν_4	ν_s	ν_l
1	$Ca_8Cd_1Pb_1(PO_4)_6(OH)_2$	955	420	1020	555	3565	—
			460	1045	560		
				1085	590		
2	$Ca_6Cd_1Pb_3(PO_4)_6(OH)_2$	940	395	1010	545	3560	—
			415	1035	585		
				1075	598		
3	$Ca_5Cd_1Pb_4(PO_4)_6(OH)_2$	940	400	1025	545	3560	665
			440	1040	560		
					600		
4	$Ca_4Cd_1Pb_5(PO_4)_6(OH)_2$	940	410	990	565	3540	655
			420	1020	590		
			465	1060			
5	$Ca_3Cd_1Pb_6(PO_4)_6(OH)_2$	940	395	1005	540	3540	655
			436	1065	580		
6	$Ca_1Cd_1Pb_8(PO_4)_6(OH)_2$	950	375	980	525	3566	655
			460	1030	560		
7	$Ca_6Cd_3Pb_1(PO_4)_6(OH)_2$	945	445	1020	545	3560	—
				1080	580		
8	$Ca_4Cd_3Pb_3(PO_4)_6(OH)_2$	940	440	1020	542	3555	650
				1085	585		
9	$Ca_5Cd_4Pb_1(PO_4)_6(OH)_2$	955	400	1010	551	3545	655
				1040	590		
				1080	600		
10	$Ca_2Cd_4Pb_4(PO_4)_6(OH)_2$	—	380	990	535	3555	660
			405	1060	570		
11	$Ca_1Cd_6Pb_3(PO_4)_6(OH)_2$	950	400	1020	545	3540	—
			410	1080	570		
12	$Ca_1Cd_8Pb_1(PO_4)_6(OH)_2$	930	380	1025	550	3566	660
			405	1065	580		

IR spectra (Table 4). The free PO_4 ion belongs to the T_d point group; it may decay either to C_{3v}, C_{2v}, or C_s symmetry when it is included in an anisotropic crystal lattice. Analysis of the number of bands makes it possible to assign each pseudotetrahedric anion to one of these symmetry groups. In this way it has been possible to study the variation of PO_4 symmetries with the substitution of Cd and Pb in CaHA. The PO_4 ion in CaHA has C_s symmetry because it shows three ν_3 and ν_4 modes, one ν_1 mode, and a doublet ν_2. The PO_4 ion in substituted apatite samples will belong either to the C_s or C_{2v} point group according to whether the number of ν_2 modes are 2 or 1 respectively (21). For substitution of Cd and Pb in the ratio 1 : 1 in CaHA the PO_4 ion belongs to the C_s point group. For samples with Cd : Pb in the ratio 1 : 3 the relative intensity of the ν_3 vibrations at 1035 cm^{-1} and of the ν_4 vibrations at 598 cm^{-1} has become very weak. This is due to the fact that a given proportion of PO_4 ions increase their symmetry from C_s to C_{3v} though the statistical average still gives a higher proportion of C_s. This symmetry group, however, is maintained over the entire compositional range thereafter.

Considering the reference value of the OH stretching frequency as 3644 cm^{-1}, the OH···O distance of the solid solutions are calculated from

$$\log (OH\cdots O) = \log 3.35 - 1/6 \log (\Delta\nu_s/50),$$

where $\Delta\nu_s$ is the difference between the OH reference frequency and ν_s the hydroxyl stretching frequency of the samples; the values are given in Table 3. The OH···O values ranged between 2.955 and 3.110 Å for all the samples including the end members, CaHA, CdHA, and PbHA. This, therefore, is indicative of a hydrogen bonding mechanism operating in the samples of CaCdPbHA that were prepared. Since the probability of the formation of a linear hydrogen bond between the OH group and the surrounding PO_4 ions is the same, it could be inferred that

TABLE 5
Frequency (in cm^{-1}) of the Cation–Oxygen Vibration and Lattice Bands of Solid Solutions of Calcium–Cadmium–Lead Hydroxylapatites

No.	Molecular formula	Cation–PO_4 lattice vibrations	Metal–Oxygen vibrations ($M \cdots OH$)		
			Ca–O	Cd–O	Pb–O
1	$Ca_8Cd_1Pb_1(PO_4)_6(OH)_2$	220,230,250	295	340	270
2	$Ca_6Cd_1Pb_3(PO_4)_6(OH)_2$	220,230,250	—	355	260,270
3	$Ca_5Cd_1Pb_4(PO_4)_6(OH)_2$	210,230,242	300,320	355	260,280
4	$Ca_4Cd_1Pb_5(PO_4)_6(OH)_2$	205,230,245	300,320	325	265,285
5	$Ca_3Cd_1Pb_6(PO_4)_6(OH)_2$	205,225,250	295,320	—	275
6	$Ca_1Cd_1Pb_8(PO_4)_6(OH)_2$	220,240,—	320	335	265
7	$Ca_6Cd_3Pb_1(PO_4)_6(OH)_2$	—,240,—	295	—	270
8	$Ca_4Cd_3Pb_3(PO_4)_6(OH)_2$	210,226,240	290	—	271
9	$Ca_5Cd_4Pb_1(PO_4)_6(OH)_2$	205,210,232	282	350	275
10	$Ca_2Cd_4Pb_4(PO_4)_6(OH)_2$	230,235,242	305	335	275
11	$Ca_1Cd_6Pb_3(PO_4)_6(OH)_2$	220,235,242	290,302	330	268,272
12	$Ca_1Cd_8Pb_1(PO_4)_6(OH)_2$	220,230,245	290,310	335	265

the OH group in the samples prepared is situated parallel to the *c*-axis.

The ν_s(OH) vibration intensity at 3576 cm^{-1} in CaHA decreases due to the substitution of (Cd + Pb) in CaHA. The progressive decrease in the cation polarization power in the order Ca < Cd < Pb contributes to the possible $OH \cdots OPO_3$ vibration and in turn to the decrease in the hydroxyl band intensities in the samples. Consequently upon substitution, the ν_1, ν_2, ν_3, and ν_4 vibrations in general are shifted to the lower side. This is due to contraction in the distance between the PO_4 groups in the lattice and introduction of covalent character owing to the greater polarizability of Cd and Pb than Ca in the apatite lattice. In all the samples the $\nu_3(PO_3)$ vibrations become broader due to various crystal fields acting on the stretching vibrations of the phosphate making the transitions less clearly defined, in addition to the stronger distortion of the PO_4 groups caused by the ordered substitution.

The absorption between 220 and 250 cm^{-1} in the IR spectra is assigned to the lattice vibrations and the bands around 265–355 cm^{-1} may be attributed to the $M \cdots O$ stretching vibrations. The oxygen atom of the $M \cdots O$ bond is that of the OH group. The frequency in cm^{-1} of the $M \cdots O$ vibrations are given in Table 5. In most cases bands are detected within 265 to 355 cm^{-1} for different proportions of Cd and Pb in the samples. The reduced masses of Ca–O, Cd–O, and Pb–O increase in the order $\mu_{Ca-O} < \mu_{Cd-O} < \mu_{Pb-O}$ and hence the lattice vibrations are expected to follow the reverse order. But the theoretical Cd–O frequency (334 cm^{-1}) is found to be greater than Ca–O (322 cm^{-1}) and Pb–O (262 cm^{-1}) consequent to the greater force constant value of Cd–O (9.22×10^4 dyn cm^{-1}) than Ca–O (7.02×10^4 dyn cm^{-1}) and Pb–O (6.09×10^4 dyn cm^{-1}) in the solid solutions, and hence is the basis of indexing the $M \cdots O$ vibrations in the IR spectra.

REFERENCES

1. P. S. Barry, *Brit. J. Ind. Med.* **32,** 119 (1975).
2. B. T. Emerson, *Australas. Ann. Med.* **12,** 310 (1968).
3. K. Tsuchiya, *J. Med.* **18,** 81 (1969).
4. S. E. Larson and M. Piscator, *Israel J. Med.* **7,** 495 (1971).
5. M. E. J. Curzon, P. C. Spector and D. C. Crocker, "Trace Substances in Environmental Health, XI" (D. D. Hemphill, Ed.), pp. 23–24.
6. E. D. Eanes and A. S. Posner, *Mater. Res. Bull.* **5,** 377 (1970).
7. E. D. Eanes and A. S. Posner, *Trans. N.Y. Acad. Sci. Ann.* **28,** 233 (1965).
8. P. W. Arnold, *Trans. Faraday. Soc.*, 1061 (1950).
9. R. L. Collin, *J. Am. Chem. Ind.* **82,** 1538 (1970).
10. V. M. Bhatanager, *Chem. Ind.* **48,** 1538 (1970).
11. T. S. B. Narasaraju, R. P. Singh, and V. L. N. Rao, *J. Inorg. Nucl. Chem.* **34,** 2072 (1972).
12. P. P. Mahapatra, H. Mishra, and N. S. Chickerur, *Proc. Natl. Acad. Sci. (India) A* **54,** 407 (1984).
13. G. Engel, *J. Solid State Chem.* **6,** 286 (1973).
14. H. J. M. Heijligers, F. C. M. Driessens, and R. M. H. Verbeeck, *Calcif. Tissue. Int.* **29,** 127 (1979).
15. A. Bigi, M. Gazzano, A. Ripamonti, E. Foresti, and N. Roveri, *J. Chem. Soc. Dalton Trans.*, 241 (1986).
16. R. M. H. Verbeeck, C. J. Lassuyt, H. J. M. Heijligers, F. C. M. Driessens, and J. W. G. A. Vrolijk, *Calcif. Tissue Int.* **33,** 243 (1981).
17. M. Andres-Verges, F. J. Higes-Rolando, C. Valenzuela-Calahorro, and P. F. Gonzalez-Diaz, *Spectrochim Acta Part A* **39,** 1077 (1983).
18. E. J. Baran and M. C. Apella, *J. Mol. Struct.* **61,** 203 (1980).
19. D. Wier, N. S. Chien, and C. A. Black, *Soil. Sci.* **III,** 107 (1971).
20. P. P. Mahapatra, D. S. Sarangi, and B. Mishra, *Indian J. Chem. Sect. A,* **32**(6), 525 (1993).
21. P. A. Galera, S. S. Pinilia, E. O. Aenlle, and P. E. Gonzalez-Diaz, *Spectrochim Acta A* **38**(2), 253 (1982).